Annual Review of Biomedical Engineering

A Theoretical Approach in Applying High-Frequency Acoustic and Elasticity Microscopy to Assess Cells and Tissues

Frank Winterroth,[1] Jing Wang,[2] Onno Wink,[1] Bart Carelsen,[1] Jeremy Dahl,[2] and Avnesh S. Thakor[2]

[1]Philips Research, Eindhoven, The Netherlands; email: frank.winterroth@gmail.com

[2]Interventional Regenerative Medicine and Imaging Laboratory, Department of Radiology, Stanford University School of Medicine, Palo Alto, California, USA

Annu. Rev. Biomed. Eng. 2025. 27:283–305

First published as a Review in Advance on February 19, 2025

The *Annual Review of Biomedical Engineering* is online at bioeng.annualreviews.org

https://doi.org/10.1146/annurev-bioeng-112823-103134

Keywords

acoustic microscopy, B-scan, C-scan, RMS data, elastography, cell/tissue imaging

Abstract

Medical ultrasound is a diagnostic imaging modality used for visualizing internal organs; the frequencies typically used are 2–10 MHz. Scanning acoustic microscopy (SAM) is a form of ultrasound where frequencies typically exceed 50 MHz. Increasing the acoustic frequency increases the specimen's spatial resolution but reduces the imaging depth. The advantages of using SAM over conventional light and electron microscopy include the ability to image cells and tissues without any preparation that could kill or alter them, providing a more accurate representation of the specimen. After scanning the specimen, acoustic signals are merged into an image on the basis of changes in the impedance mismatch between the immersion fluid and the specimens. The acoustic parameters determining the image quality are absorption and scattering. Surface scans can assess surface characteristics of the specimen. SAM is also capable of elastography, that is, studying elastic properties to discern differences between healthy and affected tissues. SAM has significant potential for detection/analysis in research and clinical studies.

Contents

1. INTRODUCTION

1.1. Background Information: Acoustic Microscopy Specifications, Applications, and Advantages

Medical ultrasound (or ultrasonography) is a common diagnostic imaging technique used to non-invasively visualize subcutaneous body structures including tendons, muscles, joints, vessels, and internal organs for possible pathology or lesions, as well as to image the developing fetus. Typical medical ultrasound frequencies range between 2 and 10 MHz. The intensity of the ultrasound

beam is defined as the concentration of energy in the beam:

$$I = \frac{P}{4\pi r^2}, \qquad 1.$$

where intensity (I) = power (P)/beam area = (amplitude)^2/beam area and is measured in watts per centimeter squared. The intensity decreases as the ultrasound propagates through tissues.

1.2. Typical Applications of Imaging Devices on Deep-Seated Organs and Tissues

In general, medical imaging systems reveal internal structures beneath skin, bone, and musculature for use in diagnosing/treating diseases. Medical imaging further is used to set up a medical image library of normal human anatomy and physiology, which can then be used to identify abnormalities caused by disease, defect, or injury. The following sections cover common imaging devices and some applications.

1.2.1. Abdominal ultrasound. An abdominal ultrasound can detect solid particulates (such as gallstones) that might impede the outflow of fluids from ducts and tubules (1). It also can image abscesses and/or cysts (1, 2).

1.2.2. Computed tomography scan with contrast dye. This imaging test identifies complications of disease such as an enclosed infection (abscess) or an accumulation of tissue and/or fluid, which may suggest abnormal conditions (3).

1.2.3. Computerized tomography: single-photon emission computed tomography and positron emission tomography. While many imaging tests show what the internal organs look like, a single-photon emission computed tomography scan can show how well the organs are working. Positron emission tomography (PET) scans may be used to evaluate the function of organs for the presence of disease or other conditions. PET is most commonly applied to detect cancer and evaluate any cancer treatment (1, 4). Other related tests that may be used to diagnose illness include abdominal X-rays, computed tomography scans of the abdomen or pancreas, and endoscopic retrograde cholangiopancreatography (5, 6).

One of the principal challenges with noninvasive imaging modalities is improving spatial resolution, particularly down to the cellular/tissue levels. Obtaining clear imaging of the tissues, and accurately assessing their physical states to characterize between healthy and affected tissues, are the key steps to early diagnosis and—in advanced imaging states—prognosticating conditions based on these physical states.

Scanning acoustic microscopy (SAM) has been employed since the 1970s—mostly in materials sciences and engineering—typically to study failure analyses and nondestructively assess structural properties. In the past two decades, it has been similarly utilized in biology and medicine to examine the structures and functions of cells and tissues. For SAM, the frequencies applied to image materials are typically greater than 50 MHz; this provides a significant dynamic range ratio between the lowest and highest values used in ultrasonic microscopy imaging.

Comparisons between the two transducers—conventional medical ultrasound and SAM—are shown in **Figure 1**. The transducers used in conventional ultrasound imaging usually consist of a handheld device with multiple elements (**Figure 1*a***)—and sometimes a servomotor—allowing simultaneous radio frequencies (RFs), which are then merged into a real-time image.

In contrast to conventional ultrasound systems, acoustic microscopes often employ a smaller transducer—similar in size to a pencil eraser—mounted on the body of the microscope (**Figure 1*b***). The scanning acoustic microscope's transducer is generally a single-element piezoelectric confocal unit, producing a signal like its conventional counterpart.

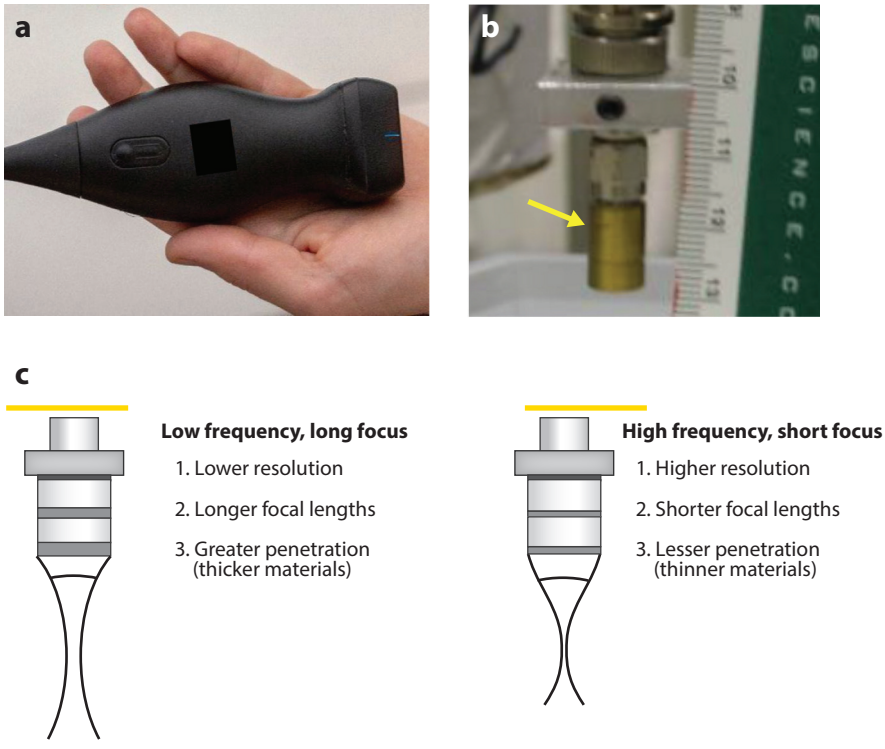

Figure 1

Comparisons between a typical handheld, multielement, linear array transducer used in standard medical ultrasound (*a*) and a single-element confocal transducer on a scanning acoustic microscope (*b*). Note that the former device is handheld, while the scanning acoustic microscope's transducer (*yellow arrow*) is mounted above the specimen stage and is approximately 3.0 mm in diameter. An illustration contrasting principal differences between the two transducer types is included (*c*).

Given such high frequencies for imaging, there is a trade-off between penetration depth of the signal through an object and spatial resolution. With higher-frequency ultrasound, there is an increased attenuation coefficient, resulting in the ultrasound wave being more readily absorbed by the material it is scanning. **Figure 1*c*** illustrates the differences between high- and low-frequency ultrasound imaging, comparing the advantages and limitations between them.

A standard SAM transducer used in imaging biological specimens operates at approximately 50–100 MHz, although in-house systems with frequencies that exceed 100 MHz do exist that are generally utilized for research (7). The parameters of SAM are generally the following:

1. scanning step size: 15 μm in both the transverse and horizontal directions,
2. axial resolution (R_{ax}): 24 μm,
3. lateral resolution (R_{lat}): 37 μm,
4. depth of field (DOF): 223 μm,
5. focal length: 4.5 mm,
6. f-number: 1.5, and
7. routine scan sampled at 300 megasamples per second.

Note: All of these parameters can be manually adjusted to accommodate a specific scan of the desired object.

R_{ax} is the resolution in the direction of propagation and is determined by the length of the ultrasound pulse propagating in the tissue, whereas R_{lat} is the resolution orthogonal to the propagation direction of the ultrasound wave. The ultrasound signal encountering the specimen has three possibilities: (*a*) scattering, where the signal travels in directions orthogonal to the transducer; (*b*) transmission, where the signal passes through the specimen; or (*c*) reflection, where the signal is received back to the transducer for processing into an image. Essentially, it is this impedance mismatch between the signal propagating through water and encountering the specimen that results in the processed image.

The sidebar titled Logistics and Formulas of the Acoustic Microscope's Operating Mechanisms and Principles provides comprehensive details of the scanning acoustic microscope's operating mechanisms, including axial and lateral resolutions, DOF, and acoustic impedance. The axial resolution depends on the dimensions of the pressure pulse, which is related to the transducer bandwidth and system electronics.

LOGISTICS AND FORMULAS OF THE ACOUSTIC MICROSCOPE'S OPERATING MECHANISMS AND PRINCIPLES

$$R_{ax} = \frac{c}{(2 \times \mathrm{BW})},$$

where c is the sound speed in the tissue and the bandwidth (BW) is 32 MHz. Likewise, the lateral resolution at the focal point can be estimated by:

$$R_{lat} = \lambda \times f\text{-number},$$

where λ is the wavelength (25 μm).

The depth of field (DOF) is calculated by:

$$\mathrm{DOF} = 4(f\text{-number})^2\lambda.$$

Due to a small f-number (which provides a tight beamwidth), the DOF is also limited.

Lateral resolution is the resolution orthogonal to the propagation direction of the ultrasound wave.

Acoustic impedance (Z): The impedance determines the amplitude of the reflected and transmitted waves at the fluid–tissue interface. Complex scattering properties of tissues are due to acoustic impedance interfaces in microstructure of tissues:

$$Z = \rho c,$$

$$R = \frac{(Z2 - Z1)}{(Z2 + Z1)},$$

where Z is the acoustic impedance, ρ is the density of the material, c is the sound speed through the material, and R is the reflection coefficient.

Acoustic radiation force impulse (ARFI) imaging is defined as follows:

$$F = \frac{2\alpha I}{c},$$

where F is the magnitude of radiation force absorption. The magnitude of radiation force from a focused ultrasound pulse in a specific spatial location is dictated by the absorption (α), the speed of sound (c) in the tissue, and the local temporal average intensity (I) of the acoustic beam. This force is in the form of a body force. Signal attenuation from scattering is negligible.

The advantages of using SAM over conventional light and electron microscopes include being able to image cells and tissues without performing any preparations (i.e., dehydration, paraffin embedment, sectioning, or staining) that could potentially kill or alter them. SAM can also provide evidence as to any degree(s) of differentiation that the cells undergo without chemically affecting their properties (8–11). In some SAM systems, there is also the ability to scan across three axes, allowing a 3D composite image of the desired specimen to be produced.

For SAM, the frequencies applied to image cells and tissues exceed 50 MHz (the usual transducer used is approximately 61 MHz). This provides a significant dynamic range ratio between the lowest and highest values used in diagnostic ultrasound. There is also the trade-off between penetration depth of the signal through an object and spatial resolution when selecting a desired frequency: Increased frequency increases resolution but reduces the depth, and vice versa. Just as in light microscopes, increasing the magnification enhances a selected area but reduces the field of view of the imaged specimen. On the flip side, increasing the frequency increases spatial resolution of the specimen but reduces the depth at which the specimen can be imaged.

2. ULTRASOUND IN IMAGING: DEFINITION, OPERATION, AND IMAGE TYPES

Medical ultrasound (or ultrasonography) is a common diagnostic imaging technique used to noninvasively visualize subcutaneous bodily structures including tendons, muscles, joints, vessels, and internal organs for possible pathology or lesions, while its most common use is in obstetrics to image the developing fetus. The frequencies often used in conventional diagnostic ultrasound—including for obstetrics—range between 2 and 10 MHz.

The most common type of 2D image achieved using conventional ultrasound is a B-mode (brightness mode) or B-scan image, which is produced from the acoustic impedance (Z) of the object being scanned by the system (12–14). The speed of sound varies as it travels through different materials and is dependent on the acoustic impedance of the material. However, the sonographic instrument assumes that the acoustic velocity (C) is constant. An effect of this assumption is that in a real body with nonuniform tissues, the beam becomes somewhat defocused and image resolution is reduced. Typical acoustic velocity in degassed/deionized water at 25°C is 1,497 m/s.

The sound from the transducer is focused by either the shape of the transducer, a lens in front of the transducer, or a complex set of control pulses originating from the ultrasound scanner, a process known as beam forming. This focusing produces an arc-shaped sound wave from the face of the transducer. The wave travels into the body and comes into focus at a desired depth.

The return of the sound wave to the transducer results in the same process as sending the sound wave, except in reverse. The returned sound wave vibrates the transducer, which converts the vibrations into electrical pulses that travel to the ultrasonic scanner, where they are processed and transformed into a digital image.

To produce an image, the ultrasound scanner must determine two factors from each received echo:

1. the difference in the time it takes for the echo to be received from the time when the sound was transmitted, and
2. the intensity of the echo.

Once the ultrasonic scanner determines these two factors, it can locate which pixel in the image to light up and to what intensity.

Transforming the received signal into a digital image may be explained by using an analogy involving a long, column-like, multilayered box. One can imagine placing a transducer at the

top of the box, sending pulses down the length of the box, and listening for any return echoes. When an echo is heard, how long it took for the echo to return is noted: The longer the wait, the deeper the layer. The strength of the echo determines the brightness setting for that layer (white for a strong echo, black for a weak echo, and varying shades of gray for everything in between). When all the echoes are recorded for the box, a composite gray-scale image can be produced.

To generate an acquired 2D ultrasound image, the ultrasonic beam is swept across the area being examined. A transducer may sweep either mechanically by rotating or manually by swinging; a 1D phased array transducer may also be used to sweep the beam electronically. The received data is processed and used to construct the image. The acquired image is then a 2D representation of the slice into the body.

3D images can be generated by acquiring a series of adjacent 2D images. Commonly, a specialized probe that mechanically scans a conventional 2D image transducer is used. However, since the mechanical scanning is slow, it is difficult to construct reliable 3D images of moving tissues. Recently, 2D phased array transducers that can sweep the beam in 3D have been developed. These can image faster and can even be used to make live 3D images of cells and tissues (15).

3. SCANNING ACOUSTIC MICROSCOPY (SAM) EFFICACY IN BIOIMAGING

SAM is an effective imaging tool to study the morphology and nonlinear elastic characteristics of tissues and biomaterials (11). It is a noninvasive and nondestructive modality that can give accurate assessments of cells and tissues while also determining the degree of differentiation that cells are undergoing in situ (5, 11, 12, 16–18). SAM has been applied to compare RF imaging between engineered and natural bioscaffolds and cells. In previous studies involving engineered oral mucosal scaffolds, cells were examined for their state of differentiation, apoptosis, and keratinization (12, 19) to determine allograft rejection rates (20). The spectral analysis results from SAM were shown to be comparable to histological counterpart images of biological specimens at different stages of growth and development.

In addition, SAM can be used to study the density and physical properties of specimens with the acoustic reflectivity from the top of a specimen used to quantify the degree of surface roughness; this was studied in our earlier experiments where we demonstrated a strong linear correlation between SAM imaging and the quantification of surface characteristics (21, 22). Such examination of the acoustic properties of tissues further provides details on their density and elasticity, as discussed below.

A scanning acoustic microscope consists of a transducer attached to a translation stage having stepper motors that control the transducer's movement in three dimensions: horizontal, transverse, and vertical. The transducer is placed beside the specimen to be imaged, which is placed in a small immersion tank. Both the transducer and specimen must be submerged in a fluid medium—usually degassed, deionized water—to couple the pressure waves into the specimen and avoid scattering from air that can be trapped between the transducer and the specimen. Given that the transducer moves in three axes, it is possible to produce composite 3D images of the specimens using a raster scan.

4. SAM: PRINCIPAL COMPONENTS

4.1. Transducer and General Design Layout

The scanning acoustic microscope's principal components are like those found on typical light microscopes: a stage and focal systems (10, 11, 23). In place of a light source and the magnifying lens,

there is often a single-element confocal transducer—approximately 3.0 mm in diameter—attached to stepper motors that control the transducer's movement in three dimensions: horizontal, transverse, and vertical. For the stage, there is also a small tank filled with degassed/deionized water where the specimen being imaged is immersed.

4.2. Specimen Setup

The desired specimen to be imaged is generally no greater than 1.0 cm^2 in area and no thicker than 3.0 mm, smaller than the focal length of the transducer. Furthermore, it must not be composed completely of material that is miscible in water after being submerged for approximately 2–3 h. Ideally, the specimen should have a density greater than water, but with most biological materials this is not the case. Therefore, a method of mounting the object either with pushpins or embedding the specimen deep into mounting clay at the base of the immersion tank is suitable. The area of the specimen being imaged must be fully exposed to the transducer.

4.3. Positioning the SAM Transducer

The tank with the specimen is positioned on the stage below the transducer and enough water is added to ensure it is approximately 1.0–2.0 mm below the rim. Mounting pins are often used, which are inserted through the object (away from the imaging area) into a softer backing, usually an adhesive sponge or mounting clay. Another method to mount the specimen requires embedding the specimen directly into mounting clay at the base of the tank, exposing the top surface of the object directly over the transducer.

5. BASIC SAM OPERATIONS: SETUP AND ACQUISITION OF STANDARD 2D IMAGES

5.1. Principal Features of SAM and Its Operation

In addition to the stage, other key features of the scanning acoustic microscope include a broadband, high-frequency pulser where the excitation signal originates and a diode expander that reduces the baseline noise before the signal travels into the transducer, where it is converted into ultrasonic waves. Signals received by the transducer go into a diode limiter, which blocks some of the high-amplitude excitation signal from the receiving electronics. The received signal is generally amplified by a set of attenuators and 32-dB fixed-gain amplifiers. Finally, the signal is captured by a high-speed 8-bit digitizing board.

A custom-built circuit takes the 10-MHz synchronized output from the digitizing board and divides it down to a 9.76-kHz square wave that triggers both the pulser and the digitizing board. The SAM signals are synchronized to reduce any signal-to-signal jitter and improve the efficiency of signal averaging. A basic illustration of the SAM signal transmission and reception is shown in **Figure 2*a***, with the principal operating units relative to the scanning acoustic microscope's overall layout.

5.2. Power and Operation

The scanning acoustic microscope consists of power supplies for both the pulser-receiver and the digitizer. Additionally, the digitizer and pulser-receiver units are typically powered on manually. A key step toward effective operation of the scanning acoustic microscope is to ensure that there are no air bubbles within the tank, including any lodged on the transducer itself. Such bubbles will cause scattering of the ultrasound waves, leading to signal attenuation and the undermining of the scanning process.

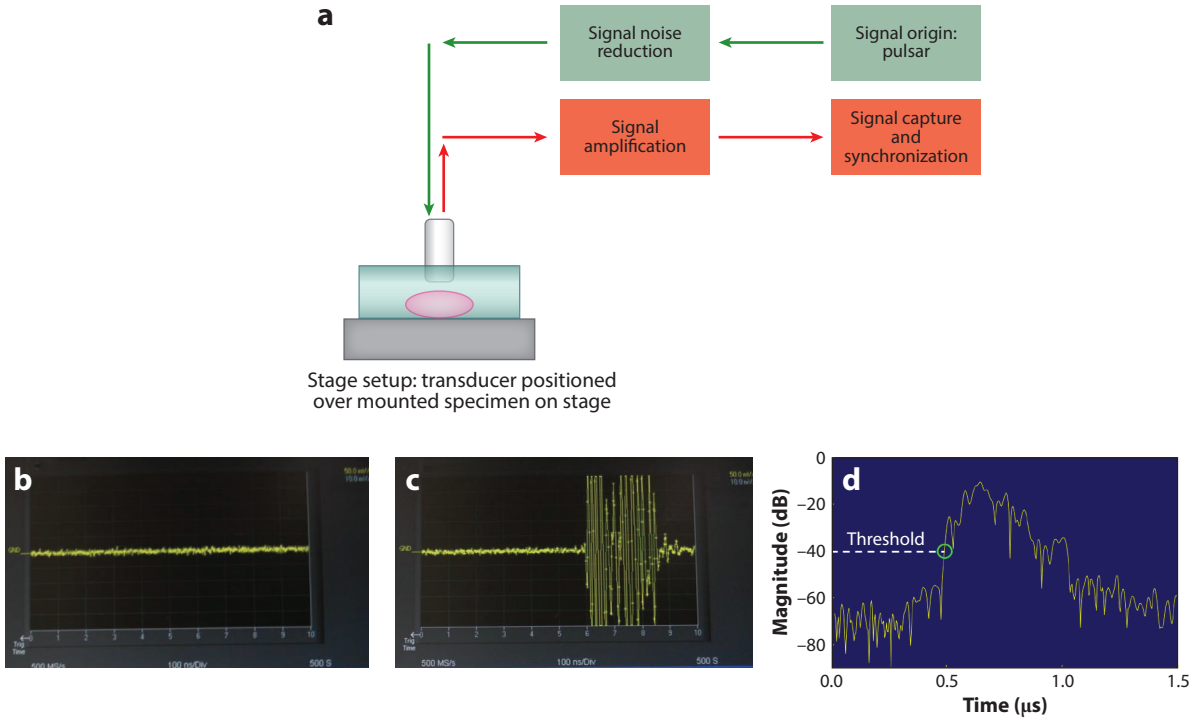

Figure 2

The principal operating units relative to the scanning acoustic microscope's overall layout (*a*). The transmitting signal originates from the pulser and undergoes noise reduction. The signal received from the specimen is amplified and captured. The scanning acoustic microscopy (SAM) signals are then synchronized to reduce any signal-to-signal jitter and improve the efficiency of signal averaging. Oscilloscope images showing the SAM background signal in water (*b*) and upon encountering the specimen (*c*). The radio-frequency (RF) signal is generated by the impedance (*Z*) mismatch between the ultrasound energy in water and the specimen. Representation of a typical acoustic envelope developed from the SAM scan of a specimen and derived from the raw RF scan (*d*). The raw scan initially includes an inverse image below zero frequency; this is eliminated by removing any frequency below zero. An inverse Fourier transform converts the scan from a frequency domain to a time domain. A threshold is set 20–30 dB above the water signal to establish the point at which the acoustic signal encounters the specimen. By examining the envelope, one can assess the thickness of the specimen—calculating the time the signal passes through—on the basis of the change in magnitude of the acoustic signal.

5.3. Image Acquisition

Once the transducer is positioned over the desired area for scanning, it is necessary to obtain the RF wave of the ultrasound. This is performed with an oscilloscope and accompanying command screen. On the command screen toolbar, the operator will select the initial/recall settings, and a command prompt will appear with the scanning acoustic microscope operation commands. After selecting the data acquisition commands, it is imperative to choose the acquisition modality, either auto or normal acquisition (one is automated, the other is manually controlled); a signal wave will then appear on the oscilloscope, with an acquisition rate of approximately 1,000–2,000/s. A trigger delay of approximately 3.0 μs is selected on the command window: This prevents the scan from "freezing" when acquiring the signal of the specimen. The operator then selects the appropriate channel of the acquisition software, which will provide a single band for the signal. This is followed by the operator making a selection to connect the data points under the tools command, which will enhance the signal coming off of the oscilloscope. At this point, a single rapid signal moving from right to left will appear on the oscilloscope (**Figure 2*b***).

5.4. Focusing the Transducer

The positioning functions of the transducer are restored, namely the Z-axis, moving the transducer in the out direction—away from the stepper motor and toward the specimen—in increments of approximately 10 steps. When the ultrasound signal encounters the specimen, an RF signal wave appears on the right-hand side of the oscilloscope (**Figure 2*c***). Here, the transducer's vertical position is adjusted so that the RF signal is in the center of the oscilloscope. Both the distance that the wave moves and the transducer's position relative to the object in the tank are examined and adjusted as needed. If the signal does not appear very strong, the attenuators can be adjusted, by clicking first on the receiving attenuator, and then on the transmitting one. The lower the number, the greater the signal increase should be. However, there will be an increase in signal noise as both the low- and high-pass filters are being reduced, and the signal is continuously adjusted until it is centered in the oscilloscope signal. Once this point on the oscilloscope is recorded, the signal is adjusted further until it attenuates. Here, it is best to zero out the position of the transducer in the vertical position, followed by reversing the adjustments made (by selecting the in direction for the Z-axis) until the signal returns to the right-hand edge of the scope. The operator records the distance traveled under the Z-axis, which is the approximate thickness of the specimen.

Once all the configurations are in place, the start key can be selected: The scope will then start scanning the desired area of the specimen. A typical scan using the parameters listed above will take approximately 20–30 min. The transducer acquires the specimen image first along the transverse line, firing 31 scans into the specimen before moving to the next point, which will be 1.25 μm × the number of steps that were entered for the scan. After scanning the desired distance along the transverse axis (usually 1.0 mm), the transducer will shift 2.5 μm × the number of selected steps in the horizontal direction and repeat scanning in the transverse direction, followed by a repeated shifting 2.5 μm × the number of selected steps in the horizontal direction and repeating in the transverse direction. The transducer follows this zigzag pattern in its scanning program until it has completed the scan over the desired area of the specimen surface. The transducer will then shift 2.5 μm × the number of steps down in the Z-direction, and the process will repeat itself.

5.5. Image Processing

Upon completing the specimen scan, the RF data is first translated into an acoustic envelope for each scan point. The raw acquired signal initially includes its inverse image, which is removed by eliminating all frequencies below zero frequency. An inverse Fourier transform is applied to convert the data from a frequency domain into a time domain. **Figure 2*d*** shows the resulting acoustic envelope of a processed signal. In this case, a threshold is set approximately 20 dB above the background noise so that the acoustic energy encountering the specimen will be displayed as the acoustic envelope.

The signals are then merged to form the image in B-mode, which is an amalgamation of the intensities of the echoes received from the transducer. The two acoustic parameters determining the image quality are absorption, which indicates how ultrasonic energy was converted into heat in the specimen, and scattering, specifically backscatter (14, 24, 25). Scattering means that an ultrasonic wave, when striking an obstacle, radiates part of its energy orthogonally to the specimen (26–31). Quantifying the degree of backscatter from small particles or perturbations in tissues and other materials allows differentiations in the degrees of pixel intensity in the B-mode images. Such scattering properties include the average scatterer (energy scattered) diameter and average scatterer concentration (29, 31).

6. BASIC OPERATIONS: KEY PRINCIPLES OF ACOUSTIC SIGNAL ACQUISITION

The principal components of acquiring the acoustic signal are described in Sections 5.1 and 5.2. A custom-built circuit takes the 10-MHz synchronized output from the digitizing board and divides it down to a 9.76-kHz square wave that triggers both the pulser and the digitizing board. SAM signals are synchronized to reduce signal-to-signal jitter and improve the efficiency of signal averaging. A detection threshold is set at 20–30 dB between the background signal of the ultrasound and the signal of the specimen being detected. An acoustic envelope of the specimen can then be produced (**Figure 2*d***).

The primary cause of acoustic attenuation in a medium such as soft tissue is absorption. Because acoustic scattering in soft tissue is weak, its contributions to attenuation can reasonably be neglected (32–34). The magnitude of the radiation force (F) from a focused ultrasound pulse in a specific spatial location is dictated by the absorption (α) and speed of sound (c) in the tissue and by the local temporal average intensity (I) of the acoustic beam (17, 24, 35):

$$F = \frac{2\alpha I}{c}. \qquad 2.$$

7. SAM IMAGING: B-SCANS AND COMPARISONS WITH CONVENTIONAL LIGHT MICROSCOPY

The most common image produced using conventional ultrasound is a 2D B-mode image from the acoustic impedance (Z) of the object being scanned (11, 30, 36); this is also known as a B-scan. It is based on the speed of sound that varies as it travels through different materials, which, in turn, is dependent on the acoustic impedance of the material. Cells and tissues are not consistently uniform in composition, structure, and density. This can lead to the acoustic beam becoming defocused, decreasing image resolution.

Table 1 provides an example of scanning logistics. It includes the number of sampling points per scan, the distances traveled by the transducer in all three dimensions, and the parameters set both manually and automatically regarding the scan (15, 16, 21, 33).

The three image types acquired by SAM constitute the ABC's of acoustics. The A-scan (or A-line) is the RF signal from a single point (x, y) in the scan. After that, it is converted into acoustic envelopes and merged into a vertical cross section, forming a B-scan. Typical C-scans are the collected data from a specified depth over the scanned area, that is, a horizontal cross section.

The typical B-scan, after acquiring and merging data from a tissue specimen, displays bright ovoid areas that represent scatter: Each is approximately 20–40 μm in diameter. **Figure 3*a*,*b*** presents B-scans contrasting two tissue specimens: One has an undeveloped surface with no cell layers (**Figure 3*a***), and the other has a fully developed cell layer on its surface (**Figure 3*b***). This is within the size range of many structural cells and white blood cells but not red blood cells, which are generally <10 μm in diameter. At 50–60 MHz, SAM can typically image a collective group of cells and tissues, equivalent to the resolution of histology images seen at 20× magnification. Development of higher-frequency transducers with accommodating digitizing boards has resulted in acoustic resolutions of subcellular components—in particular, noninvasive examination of cells undergoing apoptosis (34, 37).

Although SAM was used to study the morphology and density of skin tissue under both normal and pathologic conditions (11, 20, 38), it has not been used to gain an understanding of the growth and development of the cellular component and finalized engineered tissues during the manufacturing process, as was done in a recent study using Raman spectroscopy (12). SAM was successfully

Table 1 Typical settings and operating parameters applied to perform a standard acoustic microscopy scan

Setting/operating parameter	Description
1.555	f-Number of the transducer
3.111	Focal length of the transducer (mm)
61.0	Center of frequency of the transducer (MHz)
30.0	Bandwidth of the transducer (MHz)
31	Number of averages
256	Number of points per trace
923	Offset from the trigger
6	Number of 2.50-μm pulses between horizontal sampling points (X)
12	Number of 1.25-μm pulses between transverse sampling points (Y)
48	Number of 2.50-μm pulses between vertical sampling points (Z)
10	Number of 1.5875-μm pulses between compressor sampling points
70	Number of sites along horizontal axis (X)
70	Number of sites along transverse axis (Y)
7	Number of sites along vertical axis (Z)
1–5	Number of sites along compressor
0.50	Voltage scale (V)
14	Initial setting for transmission attenuator
14	Initial setting for reception attenuator
0.00	Voltage offset (V)
250	Sampling frequency (MHz)
3.000	Trigger level (V)
External	Trigger source
Positive	Trigger slope
9.76	Avtech repetition rate (kHz)
8	Avtech frequency setting (1–10)
7	Avtech amplitude setting (1–10)

used to assess the cellular component and final tissue properties of the tissue specimens during their growth and development (39).

8. ADVANCED SAM OPERATIONS: C-SCANS, RMS PROFILES, 3D IMAGING, AND ELASTICITY STUDIES

The C-scan is the scan along one selected horizontal-transverse plane of the specimen (22, 40, 41), most typically the surface of the specimen. Its acquisition principles resemble those of the B-scan, but the merged data is orthogonal to the data acquired in a typical B-scan. The C-scan provides surface profilometry images for all scans performed: It displays different degrees of color variation based on the quantities of surface irregularities. Images displaying large amounts of red, yellow, and blue in certain regions show greater variations in their surfaces. The classification is based on fitting the planar surface of each representative sample and subtracting any differences. **Figure 3*c*,*d*** exemplifies typical C-scans of undeveloped and fully developed tissue specimens. The greater differentiations in color represent increased irregularities in the surface of the specimen (**Figure 3*c***): All images at the plane appear in green, those above it are blue, and those below it

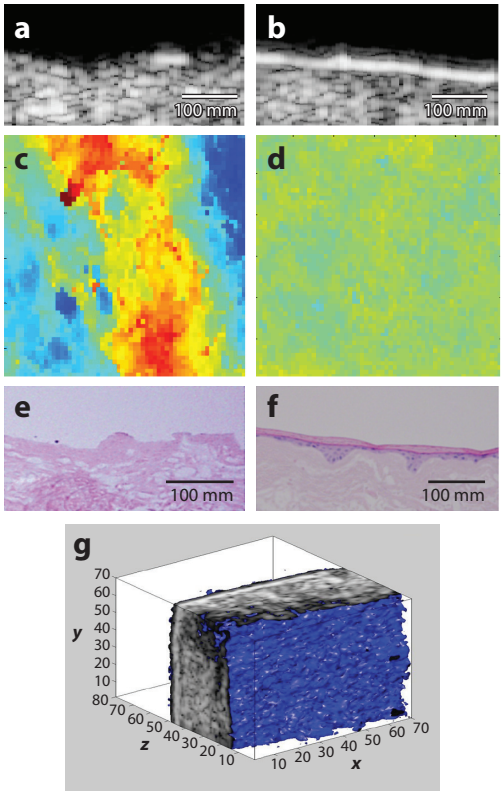

Figure 3

Scanning acoustic microscopy (SAM) B-scans, C-scans, and light microscopy images of tissue specimens, comparing undeveloped and fully developed stages. (*a*,*b*) B-scans of the tissue specimens, displaying a side view of a tissue specimen contrasting between undeveloped (*a*) and fully developed (*b*) surfaces. (*c*,*d*) C-scans, showing a top-down view of a selected area (100 μm^2) of the specimens. Note the significant color variations in panel *c*, which equate to the high presence of surface irregularities on the undeveloped specimen. In contrast, panel *d* shows a uniform yellow-green pattern, indicative of the surface being fully formed and filled in. (*e*,*f*) Light microscopy images of the undeveloped and fully developed specimens, respectively. (*g*) A 3D composite of a SAM scan showing the surface threshold, rendered in blue. All three axes indicate step sizes related to the transducer's movement over the scanning region, approximately 1.0 mm^3.

are orange/red. A C-scan of a fully developed specimen shows surface homogeneity, and higher quantities of yellow-green color indicate a more uniform surface consistency (**Figure 3*d***).

8.1. Assessing C-Scan Surface Profilometry

Surface profilometry is a method to analyze the surface conditions of the specimen, derived from a C-scan. After performing the C-scan, profilometry is determined by first finding the instance of threshold value, then fitting and subtracting the planar surface, and finally calculating the root-mean-square (RMS) height. RMS is computed in the time domain:

$$\mathrm{RMS} = \sqrt{\frac{1}{n}\sum\nolimits_n \chi^2(t)}, \qquad 3.$$

where n is the number of $x(t)$ samples. An analysis algorithm is applied to all the scans performed for each of the specimens used in this study. After detecting the front surface of each specimen and

EXAMPLE OF ACQUIRING A C-SCAN, USING A PROGRAM IN MATLAB AFTER MERGING THE ACQUIRED DATA FROM THE SCAN (FOLLOWING ACQUISITION OF A B-SCAN)

Note: These are typical image processing commands custom written as MatLab functions (and some custom sub-functions within those functions). Users of SAM must develop specific command functions such as the data files within MatLab or similar computer languages suitable for image processing.

Acquisition of the C-Scan

```
pos = ithreshold(ab,40,1:300,0),
[xn,yn] = size(pos),
[x1,y1] = meshgrid(1:yn,1:xn),
coeff = planefit(x1,y1,pos),
tilt = coeff(1)*x1+coeff(2)*y1+coeff(3),
pos2 = pos-tilt,
figure,imagescale(pos2),
colormap jet,axis image,
rms1 = ((sum(sum(pos2.^2)))/(xn*yn)).^0.5
rms2 = 1480*rms1/(2*250)
```

This previous C-Scan command will fit the planar surface and remove any tilt to the image, thus correcting for any irregularities stemming from incorrect mounting of the specimen.

subtracting any tilt, a low-pass imaging filter is applied to determine the broad underlying surface of the specimen. This filter is then subtracted from the tilt removed surface. A second filter is then applied to the resulting surface to remove any possible noise. The resulting image and RMS value are the C-scan profile: The smaller the number, the less surface variation there is on the specimen.

The sidebar titled Example of Acquiring a C-Scan, Using a Program in MatLab After Merging the Acquired Data from the Scan (Following Acquisition of a B-Scan) provides details of the processing command using MatLab to acquire a typical C-scan image. The sidebar titled Example of Processing the Acquired Images from SAM Scans, Following Acquisition of B-Scans, C-Scans, and RMS Profiles (Produced on MatLab) gives typical processing commands for the acquired images from the SAM scans, following acquisition of the B-scans, C-scans, and RMS profiles.

Figure 3*e,f* shows the light microscope counterparts (hematoxylin and eosin stained) of the acoustic B-scan images, specifically displaying side views of the undeveloped and fully developed imaged specimens.

8.2. Generating 3D Images

The 3D images are composites of the 2D B-scans produced. They are generated by compiling and merging the acquisition data multiple times. Provided that the parameters of SAM listed in Section 1.2.3 are maintained, an additional step can be performed to produce an image of the complete region that the transducer scanned.

An example of the 3D composite tissue produced using SAM is shown in **Figure 3*g***: It displays a soft tissue specimen scanned over a volume of approximately 1.0 mm^3 with the surface threshold rendered in blue. Examples of a program using software such as MatLab to acquire the images from SAM scans, converge them in the correct order, and process them are found in the **Supplemental Data**.

Supplemental Material >

EXAMPLE OF PROCESSING THE ACQUIRED IMAGES FROM SAM SCANS, FOLLOWING ACQUISITION OF B-SCANS, C-SCANS, AND RMS PROFILES (PRODUCED ON MATLAB)

Image Processing of Acquired Scans

```
for nf = 1:10 bb = merge_load6('<Enter Filename Here>',
nf,0,69,0), ab = 20*log10(abs(bb)), ab1 = ab(:,0:69,0:69),
mask1 = threshold(ab1,70,20:500,0), p1(nf) =
max(max(ithreshold(ab1,70,10:500,0))), mask2 =
threshold(ab1,60,1:700,1), ab2 = mask1.*mask2.*ab1,
view3d(ab2,1), set(gca,'CLim',[90–60,90]), fr(nf) = etframe(gcf),
clf,
end
```

9. SAM APPLICATIONS IN ELASTOGRAPHY

Elastography is a relatively new ultrasound imaging process that maps the elastic properties of incompressible soft tissue and can discern between healthy and diseased tissue types (8, 9, 25, 27, 38, 42, 43). For example, cancerous tumors will often exhibit stiffer conditions than the surrounding tissue (7, 20, 28, 43–48); elastography allows these conditions to be readily differentiated and objectively quantified.

Elastography has recently been adapted for SAM (8, 9). In SAM, elastography involves scanning before and after direct mechanical compression of the specimen and then calculating lateral displacement by the specimen to assess its degrees of stiffness/compliance under compression (9, 38). Direct physical compression to the tissues involves applying physical contact and unidirectional compression force on the tissue specimens. This is often followed by examining the rarefaction forces—resulting from viscoelastic creep—on the tissues. The degrees of changes in the stress-strain correlations (the elastic moduli for the materials being tested) account for the changes to the physical properties in the tissues.

Generally, two types of compressors are used to assess elastic properties. One compressor utilizes solid piston columns of varying sizes and applies direct force on specimens (such as incompressible tissues) to determine their displacement and viscoelastic creep (14, 49) to a known applied force. Earlier elasticity tests involved this type of mechanical compressor setup and are described in detail in previous studies (17, 23, 32, 50). Briefly, tissues are loaded onto a glass slide placed on an electronic digital scale while an in-house-built manual compressor using cylindrical pistons of different known surface areas for indentation applies compression steps. The degree of force applied with each compressive step from the piston is measured. The stress-strain correlation—and hence the elastic modulus—can be determined for the tissue specimen, at least for the bulk modulus of the tissue. However, this compression system cannot assess what specific constituents within the specimens are responsible for the major changes in elasticity (17, 49).

To obtain the Young's modulus, the slope of force–displacement response is transformed using a conversion factor. This factor is obtained experimentally and validated by finite element (FE) modeling (8, 26, 35). A piston load provides indentation in the tissue, leading to elastic deformation with the area of indentation in the same direction as the indentation forces (F). FE modeling of the object leads to the object behaving in accordance with Hooke's law:

$$F = KX, \qquad 4.$$

where K is the stiffness matrix and X is the nodal displacement.

The compressive stress (σ) is calculated by dividing the given force by the area of the piston:

$$\sigma = \frac{F}{A}. \quad 5.$$

The strain (ε) was measured as:

$$\varepsilon = \frac{\Delta L}{L_0}, \quad 6.$$

where ΔL is the change in the thickness of the specimen and L_0 is the original specimen length.

Poisson's ratio (ν) defines the relationship of transverse contraction strain to longitudinal extension strain in the direction of the stretching force. Tensile deformation is considered positive and compressive deformation is considered negative:

$$\nu = \frac{-\varepsilon_{\text{transverse}}}{\varepsilon_{\text{longitudinal}}}. \quad 7.$$

Finally, Young's modulus (E) is obtained as the ratio of stress and strain:

$$E = \frac{\sigma}{\varepsilon}. \quad 8.$$

For the indentation experiments, the piston causes displacements of equal ΔL over the given indentation area of the tissue. These compressions apply to the bulk modulus of the collective tissue specimens and cannot analyze what specific properties in the tissue—either individual or collective—account for the differences in the elastic moduli between normal and affected specimens.

Generally, soft tissue specimens with an affected condition (such as physical injury, insult, or disease) have exhibited stiffer properties, and hence a steeper stress-strain correlation. In contrast, normal specimens are more elastic and exhibit greater compliance when undergoing compression (48): A threshold in the compression is eventually reached, and the normal specimens consequently exhibit stiffer properties as observed in affected tissues' behaviors.

The second type of physical compressor utilizes SAM to analyze elastography. An example of a SAM compressor is shown in **Figure 4*a*,*b***, by itself and in use with the transducer. An illustrative side view of the transducer, the compressor, and their proximity to the specimen is shown in **Figure 4*c***. The compressor has a flat aluminum plate with a slit in the center, which is approximately 20.0 mm in length and 2.0 mm in width. After each scan volume is completed, the plate compresses the specimen a designated distance, and a successive scan is performed by SAM. A full 3D rendering of the scanned specimen at each compression step can then be produced to determine the degree of strain at specific regions of the specimen. Here, the scanning acoustic microscope is generally advantageous over the aforementioned bulk mechanical piston compressor, as it can analyze and discern what properties in the specimen contribute to the greatest or least changes in overall strain behavior (9, 10).

9.1. Acoustic Radiation Force Impulse (ARFI) Imaging and Other Noncontact Elasticity Quantification Methods

There are multiple ultrasound elastography techniques (7, 25, 45, 50). Acoustic elasticity research includes adapting noncontact deformation methods. Such noncontact stimulation accurately differentiates and/or characterizes certain tissue conditions such as lesions, apoptosis, necrosis, and sclerosis. Further, no physical contact to the specimens reduces possible alterations of the biological conditions. One noncontact method to characterize the elasticity of cells and tissues is acoustic radiation force impulse (ARFI) imaging.

ARFI utilizes focused acoustic beams to intraconvert acoustic compressional waves to shear waves through the absorption of acoustic energy (50–53). The tissues' responses to this force are monitored to assess the stiffness and/or compliance. This technology characterizes conditions of cells/tissues and quantifies to what degree they are evolving and/or affected (46). The tissue response portrays the simulated tissue displacement response to a typical impulsive acoustic

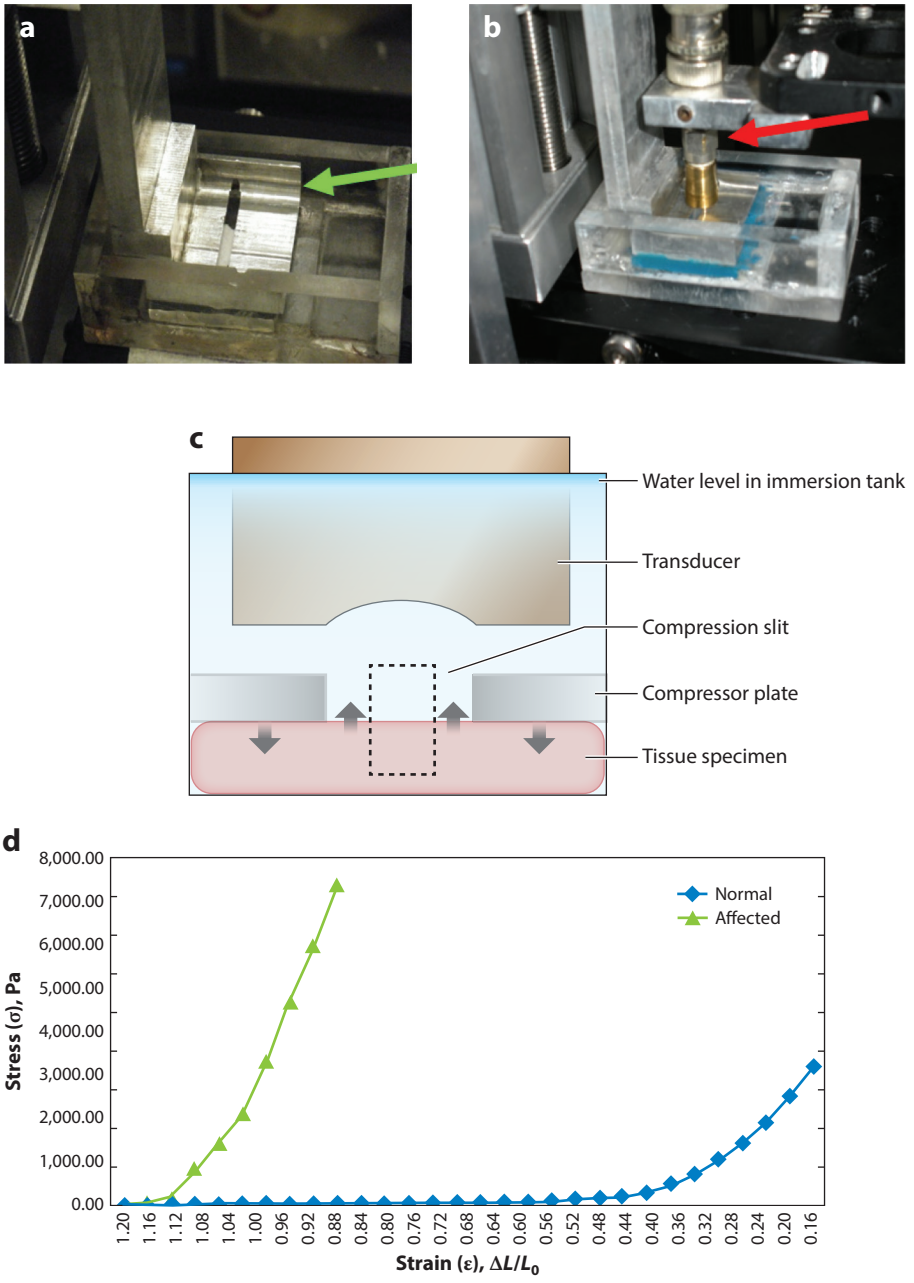

(*Caption appears on following page*)

Figure 4 (*Figure appears on preceding page*)

Photographic examples of the acoustic setup with the compressor plate (*a*) and a close-up view of the compressor plate over the tissue specimen (*b*). The specimen is immersed in degassed/deionized water with the compressor positioned directly over it. The green arrow indicates the slit opening within the plate over which the scanning acoustic microscope will scan the specimen at a selected region. The transducer (*red arrow*) is positioned over the slit opening and scans the selected tissue region at each successive compression. An illustrative schematic shows a magnified side view of the transducer, compressor, and tissue specimen (*c*). Gray downward arrows indicate the direction of the compressive forces; gray upward arrows show the direction of the tissue's subsequent displacement. The dashed black line represents the scanning area performed by the scanning acoustic microscope. Speckle tracking methods allow for a strong understanding of the degree of orthogonal displacement that the tissue undergoes during compression. An example of calculating the stiffness properties by correlating stress-strain in normal control and affected engineered soft tissues is shown (*d*). Typically, affected tissue specimens show significantly stiffer behavior when compression forces are applied, hence resulting in a very steep curve. In contrast, there is greater compliance in normal specimens during the initial compressions. Once a compression threshold is crossed, these specimens often exhibit stiffness properties that resemble the affected ones.

radiation force excitation (<1.0 ms); immediately after force application to the tissues, the displacement response reflects the distribution of the applied force. The volume and geometry of the tissue that receives the excitation force are spatially distributed throughout the area of the transducer aperture. This volume and area can vary considerably with the types of tissues being excited and their degrees of attenuation. The applied force is dependent upon the acoustic properties of the tissue.

Ultrasound induces radiation pressure along its propagation direction. This induced pressure is a body force commonly called the acoustic radiation force, a modification of Equation 1:

$$F = \frac{2\alpha I}{C}, \qquad 9.$$

where F is the force per unit volume, I is the intensity, α is the attenuation coefficient, and C is the speed of sound.

ARFI has potential for in vivo elasticity imaging (52, 53); this is a new arena of study, and its impact is mostly unknown. For most soft tissues, the primary cause of acoustic signal attenuation is absorption, and the contributions to attenuation from scattering can reasonably be neglected (7, 54).

9.2. Images Generated by ARFI

ARFI images can be formed using both commercial diagnostic ultrasound scanners and SAM: Both generate localized, impulsive acoustic radiation forces in tissues and monitor the transient, dynamic displacement tissue response within the region of excitation (ROE) using correlation-based methods. ARFI pulse sequences consist of

1. tracking beams (conventional B-mode ultrasound A-lines) and
2. pushing beams (higher intensity A-lines, with acoustic output parameters; these include the frequency range of the scanning acoustic microscope and the f-number).

A typical sequence involves transmitting a series of prepush reference A-lines, which are used to monitor underlying physiologic motion, followed by a pushing pulse along the same A-line, and then a series of tracking A-lines that are utilized to monitor the tissue displacement response within the ROE of the pushing beam (typically for 3–5 ms at pulse repetition frequencies between 5 and 10 kHz). Prepush A-lines are a reference to display underlying physiologic conditions. This is followed by a push pulse along the same A-line, then tracking A-lines to determine the response to any tissue displacement within the ROE.

Acoustic parameters are quantified using a polyvinylidene fluoride (PVDF) membrane hydrophone, with a 0.6-mm active spot size, submerged in attenuating fluid (usually a mixture of evaporated milk and water) at a concentration to achieve the desired attenuation (α) to accurately quantify the in situ intensity for radiation force and thermal calculations. The peak negative pressure measurement used to determine the mechanical index (MI) is performed in fluid with $\alpha = 0.3$ dB/cm/MHz, as prescribed by its definition. The temporal average intensity is computed using the appropriate duty cycle, which can be modulated to reduce average heating.

Other parameters include the following:

1. Spatial peak pulsed average intensity (I_{sppa}), which is the pulse average intensity, calculated at the position of the spatial maximum: mean over pulse duration.
2. Spatial peak temporal average intensity (I_{spta}), which is the temporal average intensity, calculated at the position of the spatial maximum. It is the highest intensity measured at any point in the ultrasound beam averaged over the pulse repetition period and is closely related to the magnitude of thermal bioeffects.
3. MI is an estimation of the likelihood of inertial cavitation of the biomaterial(s).
4. Power is the rate at which energy is transferred and measured in watts. This intensity is important when analyzing bioeffects of cells and tissues.

9.3. Thermal Effects from ARFI

A major factor when applying ARFI is thermal absorption of ultrasound energy by the cells/tissues, which can affect their properties. Generally, the amount of energy to displace tissue by several microns is less than what is required to raise its temperature by a fraction of a degree Celsius (34). Two principal unknowns exist that can potentially change thermal elevation: (*a*) how much displacement is required to quantify, compare, and distinguish stiffness differences between normal and affected (i.e., necrotic, malignant) tissues; and (*b*) whether such displacement using ARFI elevates tissue temperature enough to affect the properties of cells/tissues—both normal and affected (30). How much integrity of the cells and tissues remains after ARFI applications—considering the number of applications, the application lengths, and the application intensities—reflects how effective the scanning acoustic microscope is as a diagnostic and prognostic medical instrument.

2D and 3D ARFI images display tissue displacement at a given time after force application, the maximum tissue displacement, the time the tissue takes to reach its peak displacement, and the time it takes the tissue to recover (48). The magnitude of tissue displacement correlates to the tissue structure and its underlying stiffness. Displacement and recovery time of the tissues further quantify their stiffness (31, 55–58).

Quantifying elastography using SAM involves applying the aforementioned compression/rarefaction forces on the specimens and correlating changes in stress-strain. The most prominent of these methods include quasistatic elastography/strain imaging, shear wave elasticity imaging, supersonic shear imaging, and transient elastography (48, 57–60).

Mechanical stimulation of tissues is performed by either external static compression (i.e., strain imaging), external dynamic vibration (i.e., sonoelasticity, transient elastography), or naturally occurring physiologic motion (i.e., cardiac strain-rate imaging). Current elastography requires stimulating the tissue and observing its response (48, 49).

For these compression experiments, the piston causes displacements of equal ΔL over the given indentation area of the tissue. These compressions apply to the bulk modulus of the collective tissue specimens and cannot analyze what specific properties in the tissue—either individual or collective—account for the differences in the elastic moduli between normal and affected specimens.

SAM systems have been applied to obtain elastic properties, such as Young's modulus, in different soft tissues, including cardiac and cornea (10, 28, 32–34, 50), natural or engineered oral mucosal tissues (44), and skin tissue (8, 59). Skin tissue exhibits similar morphology to mucosal tissues because they are derived from the same embryological tissues.

Figure 4*d* gives an example of correlating and comparing stress-strain curves between normal and affected engineered tissue specimens when subjected to compression forces. In this context, affected means that some tissues were subjected to a physical insult (i.e., temperature elevation, pH imbalance, change in the growth media) to deliberately alter their characteristics prior to the compressions. Typically, affected tissue specimens show significantly stiffer behavior when compression forces are applied, hence resulting in a very steep curve. In contrast, there is greater compliance in normal specimens during the initial compressions, and little to no change in the stress-strain correlation. Once a compression threshold is crossed, these specimens often exhibit stiffness properties that resemble affected tissues, resulting in a steep stress-strain curve.

Previous studies demonstrated the different stiffness characteristics—based on stress-strain values—between transitional and fully developed tissue specimens (32, 39, 40). More recent studies show which specific sites in each of the tissues contribute the most to the strain measurements. This will provide greater analyses as to what properties in the cells and tissues contribute to the differences between the healthy controls and diseased specimens (such as cancerous specimens) (43, 47, 50, 51, 61). These experiments are essential to learn how ultrasound can aid in understanding the physical properties of different tissues.

10. FUTURE DIRECTIONS: SAM AS A POTENTIAL DIAGNOSTIC TOOL

Developing new tools and techniques to accurately assess organs/tissues in the earliest stages of specific conditions is critical to predict long-term outcomes and provide the most successful medical interventions. Examining the earliest stages of inflammatory, apoptotic, and necrotic conditions of organs and tissues is the most effective way to accurately correlate such conditions to predicted outcomes (32, 56). Specifically, showing causations among these tissues and prognosticating their subsequent effects is prudent for developing the earliest possible interventional therapy.

Examining internal organs and tissues for conditions that could improve diagnostic procedures could lead to advancements in early treatment methods. The scanning acoustic microscope's ability to assess normal versus affected conditions of tissues might make it a suitable device to contribute to these overall improvements.

Acoustic microscopy has a proven ability to accurately and objectively image and quantify structural characteristics of cells and tissues (18, 21, 22, 40, 60, 62). This makes it an ideal biomedical tool to identify and assess the conditions of organs/tissues. Testing biopsy specimens for their elastic characteristics, objectively analyzing their stiffness and/or compliance, and comparing these results with healthy control specimens are essential first steps toward determining their conditions: normal versus pathological (22, 40). The scanning acoustic microscope's ability to characterize elasticity features in cells/tissues makes it an exceptional tool in such diagnoses.

DISCLOSURE STATEMENT

A.S.T. is a member of the advisory boards of RespondHealth, TealHealth, Cellular Vehicles, Nephrogen, ReThink 64, and Allo TRx and is a paid consultant for Genentech and Inari Medical.

ACKNOWLEDGMENTS

We gratefully acknowledge the National Institutes of Health Resource Center for Medical Ultrasonic Transducer Technology at the University of Southern California (Los Angeles, CA) for designing and building the high-frequency transducer used in this study. We also thank Dr. Stephanie Schampaert at Philips Medical Systems (Netherlands) for her kind support of this work.

LITERATURE CITED

1. Wang Z, Chen JQ, Liu JL, Qin XG, Huang Y. 2013. FDG-PET in diagnosis, staging and prognosis of pancreatic carcinoma: a meta-analysis. *World J. Gastroenterol.* 19:4808–17
2. Rickes S, Unkrodt K, Neye H, Ocran KW, Wermke W. 2002. Differentiation of pancreatic tumors by conventional ultrasound, unenhanced and echo-enhanced power Doppler sonography. *Scand. J. Gastroenterol.* 37:1313–20
3. Kittaka H, Takahashi H, Ohigashi H, Gotoh K, Yamada T, et al. 2013. Role of ^{18}F-fluorodeoxyglucose positron emission tomography/computed tomography in predicting the pathologic response to preoperative chemoradiation therapy in patients with resectable T3 pancreatic cancer. *World J. Surg.* 37:169–78
4. Tang S, Huang G, Liu J, Liu T, Treven L, et al. 2011. Usefulness of 18F-FDG PET, combined FDG-PET/CT and EUS in diagnosing primary pancreatic carcinoma: a meta-analysis. *Eur. J. Radiol.* 78:142–50
5. Adamek HE, Albert J, Breer H, Weitz M, Schilling D, Riemann JF. 2000. Pancreatic cancer detection with magnetic resonance cholangiopancreatography and endoscopic retrograde cholangiopancreatography: a prospective controlled study. *Lancet* 356:190–93
6. Tummala P, Junaidi O, Agarwal B. 2011. Imaging of pancreatic cancer: an overview. *J. Gastrointest. Oncol.* 2:168–74
7. Parker KJ, Doyley MM, Rubens DJ. 2011. Imaging the elastic properties of tissue: the 20 year perspective. *Phys. Med. Biol.* 56(1):R1–29. Corrigendum. 2011. *Phys. Med. Biol.* 56(2):513. Corrigendum. 2012. *Phys. Med. Biol.* 57(16):5359–60
8. Amelink A, Kaspers OP, Sternborg HJCM, van der Wal JE, Roodenburg JLN, Witjes MJH. 2008. Noninvasive measurement of the morphology and physiology of oral mucosa by use of optical spectroscopy. *Oral Oncol.* 44:65–71
9. Bathe K-J. 1996. *Finite Element Procedures*. Hoboken, New Jersey: Prentice-Hall
10. Briggs A, Kolosov O. 2009. *Acoustic Microscopy*. Oxford, UK: Oxford Univ. Press. 2nd ed.
11. Broekaert D, Van Oostveldt P. 1988. Nuclear differentiation during epidermal keratinization. *Arch. Dermatol. Res.* 280:188–89
12. Khmaladze A, Ganguly A, Kuo S, Raghavan M, Kainkaryam R, et al. 2013. Tissue-engineered constructs of human oral mucosa examined by Raman spectroscopy. *Tissue Eng. Part C Methods* 19:299–306
13. Kolios MC, Czarnota GJ, Lee M, Hunt JW, Sherar MD. 2002. Ultrasonic spectral parameter characterization of apoptosis. *Ultrasound Med. Biol.* 28:589–97
14. Kolios MC, Taggart L, Baddour RE, Foster FS, Hunt JW, et al. 2003. An investigation of backscatter power spectra from cells, cell pellets, and microspheres. In *IEEE Ultrasonics Symposium*, pp. 752–57. New York: IEEE
15. Muenier J. 1987. Tissue motion assessment from 3D echographic speckle tracking. *Phys. Med. Biol.* 43:1241–54
16. Cohn NA, Emelianov SY, Lubinski MA, O'Donnell M. 1997. An elasticity microscope. Part I: methods. *IEEE Trans. Ultrason. Feroelectr. Freq. Control* 44(6):1304–19
17. Cohn NA, Emelianov SY, O'Donnell M. 1997. An elasticity microscope. Part II: experimental results. *IEEE Trans. Ultrason. Feroelectr. Freq. Control* 44(6):1320–31
18. Samani A, Bishop J, Luginbuhl C, Plewes DB. 2003. Measuring the elastic modulus of ex vivo small tissue samples. *Phys. Med. Biol.* 48(14):2183–98
19. Somekh MG, Bertoni HL, Briggs GAD, Burton NJ. 1985. A two-dimensional imaging theory of surface discontinuities with the scanning acoustic microscope. *Proc. R. Soc. Lond. Ser. A Math Phys. Sci.* 401:29–51

20. Moll R, Divo M, Langbein L. 2008. The human keratins: biology and pathology. *Histochem. Cell Biol.* 129:705–33
21. Winterroth F, Kato H, Kuo S, Feinberg SE, Hollister SJ, et al. 2014. High frequency ultrasonic imaging of growth and development in manufactured engineered oral mucosal tissue surfaces. *Ultrasound Med. Biol.* 40(9):2244–51
22. Winterroth F, Lee J, Kuo S, Fowlkes JB, Feinberg SE, et al. 2011. Acoustic microscopy analyses to determine good versus failed tissue engineered oral mucosa under normal or thermally stressed culture conditions. *Ann. Biomed. Eng.* 39(1):44–52
23. Czarnota GJ, Kolios MC, Vaziri H, Benchimol S, Ottensmeyer FP, et al. 1997. Ultrasonic biomicroscopy of viable, dead, and apoptotic cells. *Ultrasound Med. Biol.* 23:961–65
24. Holland MR, Hall CS, Lewis SH, Handley SM, Finch-Johnston AE, et al. 1997. Comparison of integrated backscatter values obtained with acoustic densitometry with values derived from spectral analysis of digitized signals from a clinical imaging system. *J. Am. Soc. Echocardiogr.* 10(5):511–17
25. Matsuyama T, St. Goar FG, Tye TL, Oppenheim G, Schnittger I, Popp RL. 2003. Ultrasonic tissue characterization of human hypertrophied hearts in vivo with cardiac cycle-dependent variation in integrated backscatter. *Circulation* 80:925–34
26. Hughes TJR. 2000. *The Finite Element Method: Linear Static and Dynamic Finite Element Analysis*. Mineola, NY: Dover Publ.
27. Lubinski MA, Emelianov SY, Raghavan KR, Yagle AE, Skovoroda AR, O'Donnell M. 1996. Lateral displacement estimation using tissue incompressibility. *IEEE Trans. Ultrason. Feroelectr. Freq. Control* 43:247–56
28. Lynch SM, Vrieling A, Lubin JH, Kraft P, Mendelsohn JB, et al. 2009. Cigarette smoking and pancreatic cancer: a pooled analysis from the Pancreatic Cancer Cohort Consortium. *Am. J. Epidemiol.* 170:403–13
29. Matsuyama T, Valantine HA, Gibbons R, Schnittger I, Popp RL. 1990. Serial measurement of integrated ultrasonic backscatter in human cardiac allografts for the recognition of acute rejection. *Circulation* 81:829–39
30. Nightingale K. 2011. Acoustic radiation force impulse (ARFI) imaging: a review. *Curr. Med. Imaging Rev.* 7(4):328–39
31. Zuber M, Gerber K, Erne P. 1999. Myocardial tissue characterization in heart failure by real-time integrated backscatter. *Eur. J. Ultrasound* 9:135–43
32. Gandolfi L, Torresan F, Solmi L, Puccetti A. 2003. The role of ultrasound in biliary and pancreatic diseases. *Eur. J. Ultrasound* 16:141–59
33. Hollman KW, Shtein RM, Tripathy S, Kim K. 2013. Using an ultrasound elasticity microscope to map three-dimensional strain in a porcine cornea. *Ultrasound Med. Biol.* 39(8):1451–59
34. Hollman KW, Emelianov SY, Neiss JH, Jotyan G, Spooner GJR, et al. 2002. Strain imaging of corneal tissue with an ultrasound elasticity microscope. *Cornea* 21(1):68–73
35. Harrison CA, Gossiel F, Layton CM, Bullock AJ, Johnson T, et al. 2006. Use of an in vitro model of tissue engineered skin to investigate the mechanism of skin graft contraction. *Tissue Eng.* 12:3119–33
36. Iglesias-Garcia J, Lindkvist B, Lariño-Noia J, Abdulkader-Nallib I, Dominguez-Muñoz JE. 2017. Differential diagnosis of solid pancreatic masses: contrast-enhanced harmonic (CEH-EUS), quantitative-elastography (QE-EUS), or both? *United Eur. Gastroenterol. J.* 5:236–46
37. Coppola JM, Ross BD, Remtulla A. 2008. Non-invasive imaging of apoptosis and its application in cancer therapeutics. *Clin. Cancer Res.* 14(8):2492–501
38. Barr RJ, White GM, Jones JP, Shaw LB, Ross PA. 1991. Scanning acoustic microscopy of neoplastic and inflammatory cutaneous tissue specimens. *J. Investig. Dermatol.* 96:38–42
39. Ophir J, Céspides I, Ponnekanti H, Li X. 1991. Elastography: a quantitative method for imaging the elasticity of biological tissues. *Ultrason. Imaging* 13(2):111–34
40. Winterroth F, Hollman KW, Kuo S, Ganguly A, Feinberg SE, et al. 2013. Characterizing morphology and nonlinear elastic properties of normal and thermally stressed engineered oral mucosal tissues using scanning acoustic microscopy (SAM). *Tissue Eng. Part C Methods* 19(5):345–51
41. Xi X, Li X, Miyasaka C, Kropf M, Tittmann BR. 2013. High frequency scanning acoustic microscopy as diagnostic tool in tissue science. *J. Biotechnol. Biomater.* 3:160

42. Tersmette AC, Petersen GM, Offerhaus GJ, Falatko FC, Brune KA, et al. 2001. Increased risk of incident pancreatic cancer among first-degree relatives of patients with familial pancreatic cancer. *Clin. Cancer Res.* 7:738–44
43. Jemal A, Siegel R, Xu J, Ward E. 2010. Cancer statistics, 2010. *CA Cancer J. Clin.* 60:277–300
44. O'Donnell M, Bauwens D, Mimbs JW, Miller JG. 1979. Broadband integrated backscatter: an approach to spatially localized tissue characterization in vivo. In *IEEE Ultrasonics Symposium*, pp. 175–78. New York: IEEE
45. Lowenfels AB, Maisonneuve P, Cavallini G, Ammann RW, Lankisch PG, et al. 1993. Pancreatitis and the risk of pancreatic cancer. *N. Engl. J. Med.* 328:1433–37
46. Martin K. 2010. Introduction to B-mode imaging. In *Diagnostic Ultrasound: Physics and Equipment*, *Second Edition*, ed. P Hoskins, K Martin, A. Thrush, pp. 11–30. Cambridge, UK: Cambridge Univ. Press
47. Hirshberg Found. Pancreat. Cancer Res. 2024. Pancreatic cancer facts. *Hirshberg Foundation for Pancreatic Cancer Research*. **http://pancreatic.org/pancreatic-cancer/pancreatic-cancer-facts/**
48. O'Donnell M, Skovoroda AR, Shapo BM, Emelianov SY. 1994. Internal displacement and strain imaging using ultrasonic speckle tracking. *IEEE Trans. Ultrason. Feroelectr. Freq. Control* 41:314–25
49. Erkamp RQ, Wiggins P, Skovoroda AR, Emelianov SY, O'Donnell M. 1998. Measuring the elastic modulus of small tissue samples. *Ultrason. Imaging* 20(1):17–28
50. Fenner J, Stacer AC, Winterroth F, Johnson TD, Luker KE, Luker GD. 2014. Macroscopic stiffness of breast tumors predicts metastasis. *Nat. Sci. Rep.* 4:5512
51. Revell J, Mirmehdi M, McNally D. 2005. Computer vision elastography: speckle adaptive motion estimation for elastography using ultrasound sequences. *IEEE Trans. Med. Imaging* 24(6):755–66
52. Rognin N, Unnikrishnan S, Klibanov AL. 2013. *Molecular ultrasound imaging enhancement by volumic acoustic radiation force (VARF): pre-clinical in vivo validation in a murine tumor model*. Poster presented at the World Molecular Imaging Congress, Savannah, GA, Sep. 20
53. Wells PNT. 2011. Medical ultrasound: imaging of soft tissue strain and elasticity. *J. R. Soc. Interface* 8(64):1521–49
54. Szabo TL. 2014. *Diagnostic Ultrasound Imaging: Inside Out*. Boston: Elsevier Science. 2nd ed.
55. Yoder JH, Elliot DM. 2010. Nonlinear and anisotropic tensile properties of graft materials used in soft tissue applications. *Clin. Biomech.* 25:378–82
56. Zhang L, Sanagapalli S, Stoita A. 2018. Challenges in diagnosis of pancreatic cancer. *World J. Gastroenterol.* 24(19):2047–60
57. Lubinski MA, Emelianov SY, O'Donnell M. 1999. Speckle tracking methods for ultrasonic elasticity imaging using short time correlation. *IEEE Trans. Ultrason. Feroelectr. Freq. Control* 46:82–96
58. Saijo Y, Miyakawa T, Sasaki H, Tanaka M, Nitta S. 2004. Acoustic properties of aortic aneurysm obtained with scanning acoustic microscopy. *Ultrasonics* 42:695–98
59. Dill-Müller D, Maschke J. 2007. Ultrasonography in dermatology. *J. Dtsch. Dermatol. Ges.* 5:689–707
60. Sarvazyan A, Hall TJ, Urban MW, Fatemi M, Aglyamov SR, Garra BS. 2011. Overview of elastography—an emerging branch of medical imaging. *Curr. Med. Imaging Rev.* 7(4):255–82
61. Schnelldorfer T, Ware AL, Sarr MG, Smyrk TC, Zhang L, et al. 2008. Long-term survival after pancreatoduodenectomy for pancreatic adenocarcinoma: Is cure possible? *Ann. Surgery* 247:456–62
62. Saijo Y, Tanaka M, Okawai H, Dunn F. 1991. The ultrasonic properties of gastric cancer tissues obtained with a scanning acoustic microscope. *Ultrasound Med. Biol.* 17(7):709–14